Self-Diffusivity Estimation by Molecular Dynamics

ARTICLE *in* INDUSTRIAL & ENGINEERING CHEMISTRY RESEARCH · APRIL 2010

Impact Factor: 2.59 · DOI: 10.1021/ie901247k

2 AUTHORS:

Z. Nevin Gerek
Schneider Electric, Lake Forest, CA
22 PUBLICATIONS **280** CITATIONS
SEE PROFILE

Jarrell Richard Elliott
University of Akron
100 PUBLICATIONS **1,154** CITATIONS
SEE PROFILE

Self-Diffusivity Estimation by Molecular Dynamics

Z. Nevin Gerek and J. Richard Elliott*

Department of Chemical and Biomolecular Engineering, The University of Akron, Akron, Ohio 44325-3906

Reference fluid simulations are combined with a mean field correction for attractive effects to achieve a correlation for diffusivity of unentangled species over a wide range of density, temperature, and molecular weight. Reference fluids are composed of hard united atom descriptions including branching, rings, bond angles, and chain length. The molecular model is consistent with the one studied previously by thermodynamic perturbation theory. Molecular simulations of methane through triacontane provide the basis for a diffusivity correlation of reference *n*-alkanes from zero density to the glass transition. The low density limit is shown to exhibit Rouse scaling, contradicting typical hard sphere models. Experimental data for *n*-alkanes ranging from methane to hexadecane are used to correlate the correction for attractive forces and for the softness of the potential function. The average deviation is 8.6% for 657 data points. Reference simulations of nonalkanes show that the reference simulations can be interpolated smoothly with the *n*-alkane correlation by treating the effective chain length as an adjustable parameter. Applying the corresponding alkane mean field correction for attractive forces results in poor predictions for nonalkanes. The attractive energy must be treated as a single adjustable parameter to achieve reasonable accuracy. Existing correlations require two parameters to achieve comparable accuracy, and the physical meaning of the two parameters is difficult to interpret. A correlation between diffusivity and entropy suggested by Rosenfeld is shown to be problematic for chain molecules. Overall, diffusivity data are treated for 35 compounds with 1801 data points with 14% deviation by the correlation developed here.

1. Introduction

Diffusivity is an important property in the design of processes involving mass transfer. Transport models of distillation, finite element models of reactors, and even simple models of membrane transport require diffusivity estimates. Furthermore, the trends in reciprocal viscosity are similar to those of diffusivity with respect to density, temperature, and molecular weight, suggesting the possibility of predicting the viscosity from diffusivity. Also, diffusivity may provide a reasonable basis for estimating the friction parameter in coarse grained methods like Langevin equations. Unfortunately, experimental studies of self-diffusivity have been few in comparison to studies of viscosity and thermal conductivity. Available data in the literature cover limited substances and a limited portion of the fluid region. These considerations motivate the development of a generalized methodology for predicting diffusion coefficients.

Besides the scarcity of experimental data, there is a dearth of engineering correlations capable of estimating diffusivity for dense fluids of high molecular weight and gases under high pressure conditions in a manner that is consistent with the well-established methods for low density gases. Most of the correlation efforts have focused on extrapolating results for spherical molecules like methane to larger and more complex molecules like hexadecane or chlorobenzene. The methods of Liu et al.[1] and Zabaloy et al.[2] are typical of these methods and form a basis of comparison to existing methodology. Not surprisingly, the accuracy of such an approach deteriorates as the molecular complexity increases. An alternative correlation methodology has been reported by Yu and Gao[3] based on tangent sphere (TS) chain simulations. Their correlation characterizes the repulsive friction in terms of an equivalent tangent sphere chain then empirically treats the attractive friction. Owing to the indirect connection between the assumed molecular model (i.e., spheres or TS chains) and the molecules themselves (i.e., fused-sphere chains, rings, branches), the existing methods are generally applied as specific correlations for each compound rather than as generalized correlations with predictive capability. Since our goal is to develop a generalized predictive methodology, we must generalize the existing methods as much as possible to facilitate comparisons.

Molecular dynamics (MD) simulation offers the prospect of accounting for details of the molecular complexity while providing rigorous estimates of the diffusivity. The diffusivity is the simplest transport property to track by MD. With progress in computational speed and simulation alogorithms, it is natural to consider MD as a basis for generalized prediction and correlation. Previous efforts to implement MD have focused primarily on phenomenology. Grest and co-workers[4] have studied the diffusivity of tangent soft sphere chains, Hall and co-workers[5] have studied tangent hard sphere chains, and Theodorou and co-workers[6−8] have studied more realistic united atom Lennard-Jones (UA-LJ) chains. Collectively, these works establish that MD simulation is capable of mimicking the phenomenology of diffusivity, including changes in scaling with changes in molecular weight.

On the other hand, the previous work on phenomenology does not provide a direct comparison of the accuracy of MD relative to existing engineering correlations for a broad range of molecular types and complexity. Rowley and co-workers[9] developed an analytical equation as a function of temperature and density for self-diffusivity and viscosity based on simulations of a Lennard-Jones fluid. They have performed preliminary comparisons to experimental data with this goal in mind. They demonstrated accuracy of 5.3% compared to the experimental viscosity of argon. Cummings and co-workers[10] studied self-diffusivity of squalane at two different temperatures. They achieved an accuracy of 30% for squalane. Daivis et al.[11] studied diffusivity of liquid butane near the boiling point ($T = 291.6$ K and $\rho = 0.583$ g/cm^3). They achieved accuracy for butane at

* To whom correspondence should be addressed. E-mail: jelliott@uakron.edu.

10.1021/ie901247k

one specified point of 9%. Dysthe et al.[12] obtained similar accuracy of 10% for *n*-butane at the same state point. They extended their simulations to predict diffusivities of *n*-butane, *n*-decane, *n*-hexadecane, and 2-methylbutane at different state points using different united atom (UA) interaction potential models. Each potential model provided different values and overall average deviation error from the experimental data was 41% for *n*-decane and 42% for *n*-hexadecane.[13]

The potential functions in all these cases were developed to match thermodynamic properties like liquid density and solubility parameter, meaning that the computed diffusivities were truly predictions. While it would be desirable from a predictive perspective to obtain high accuracy from potentials developed based entirely on thermodynamic properties, transport properties may be sensitive to different details of the potential model. Higher accuracy might be achieved by combining the insights from MD with the analysis of experimental data. In this way, empiricism and molecular simulation can serve complementary roles to the full advantage of engineers interested in accurate physical property predictions.

The particular objective of the present work is to develop a correlation for self-diffusion coefficient that is founded on MD simulation using transferable potential functions based on the thermodynamic properties of a wide range of compounds. Trajectories of all the atoms over time are an incidental part of the MD simulation required for thermodynamics, and we would like to understand the most effective use that can be made of that information. The specific MD implementation of interest is the step potential equilibria and discontinuous molecular dynamics (SPEADMD) model.[14,15] An inherent feature of the SPEADMD model is that detailed simulations are performed for the reference potential only. To clarify, the step potentials of SPEADMD include an infinite repulsive step that represents the repulsive core and a sequence of outer steps (typically four) that characterize disperse attractive forces. Previous research has shown that thermodynamic perturbation theory (TPT) can provide quantitative accuracy in characterizing the thermodynamic contributions of the attractive wells.[16] This means that only the repulsive reference system needs to be simulated in detail. Note that the reference system does include details of molecular complexity like size, shape, and branching. Simulations of just the reference potential can be performed at least 10 times faster than simulations of the full potential, making the methodology more practical for engineering applications. Hence, the present work extends the perspective of the SPEADMD model to include transport properties as well as thermodynamic properties.

Unfortunately, no rigorous perturbation theory comparable to TPT exists for transport properties. For the present work, the lack of a rigorous perturbation theory for diffusivity is both a curse and a blessing. Since we seek to characterize an empirical contribution to the reduced diffusivity (D/D^{ref}) where D^{ref} is the diffusivity of the reference system, the lack of a rigorous result leaves open the possibility of empirically correlating the contribution in the form of a perturbation expansion. Our approach is similar to that of Yu and Gao, except that we assume the rigorous MD simulation of the reference system as the starting point, instead of the TS chain.

To develop a generalized methodology for predicting diffusivity based on molecular dynamics simulation, we first establish a foundation for a broad range of molecular weights. Thus we begin in section 1 by studying qualitative trends with TS chain fluids, including the entanglement region, to validate our simulation capability relative to existing literature. These results establish that MD is capable of characterizing scaling transitions that Enskog theory cannot. A similar analysis in section 2 is extended to repulsive reference models of fused sphere *n*-alkane chains to make contact with more realistic molecular models. Section 3 develops a generalized correlation for *n*-alkanes (C1−C16) that incorporates the effects of attractive forces through a perturbation perspective and describes a small adjustment to account for the softness of molecular interactions at high temperature. The result correlates experimental data for *n*-alkanes to roughly 9% error. Attempts are made to generalize the existing methods for a consistent comparison. Section 4 describes how the correlation for *n*-alkanes establishes a reference system that can be applied more broadly to molecules including branches, rings, and hydrogen bonding. We find that predictive accuracy deteriorates in the broader application, which we attribute to the widely variable nature of the attractive forces in nonalkanes. Reasonable accuracy can be recovered by characterizing the attractive energy with a single parameter, resulting in a specific correlation. Once again, this correlation is compared to existing methods using a consistent database and generalizing as much as possible.

2. Self-Diffusivity of Hard Fused Sphere Chains

Diffusivities of hard sphere fluids have been studied by MD since the initial work of Alder et al.[17] While the findings have not changed qualitatively, precise details vary with system size and the duration of the simulations.[5,18] The same methodology can be extended to investigate the diffusivity behavior of tangent sphere chain fluids. Self-diffusivities were calculated in the center of mass reference frame using the Einstein approach defined in eq 1.

$$D = \lim_{t\to\infty} \frac{\langle(\Delta r)^2\rangle}{6t} \tag{1}$$

where Δr is the displacement in the particle's coordinates after a time of t. Uncertainties in D were estimated by recomputing diffusivity with various intervals (10 and 25 ps update times) and taking the averages. Uncertainties tend to be higher for longer chains because relatively short simulation time was used to compute diffusion coefficients. In general, the molecules should move through a distance at least 10 times their radius of gyration (r_G) in order to achieve a reasonably accurate measure of their diffusivity. Not only do larger molecules have larger radii of gyration, but they also move more slowly so the time simulated must be larger. Furthermore, the computation time increases for a fixed number of molecules at a fixed time simulated because the number of sites increases. For the largest molecules in this study, at the highest densities, the simulation times barely comply with this guideline while, for the smaller molecules, the guideline is satisfied many times over.

Simulations were performed at 300 K for 10−20 ns each. System sizes consisted of 100 molecules for C1−C16 and 32 molecules for larger chains. Naturally, this means that the precision is reduced for the simulations of the longest chains. To improve precision, diffusivity results were computed over multiple 6 ns windows and averaged. Figure 1 shows a plot of mean squared displacement versus time for *n*-hexane at three packing fractions. It is clear that the displacements for *n*-hexane are near 1000 r_G, even at the highest density.

The diameters of each site are listed in Table 1. Bonded interactions were defined by $L_{12} = 0.151 \pm 0.0076$ nm, $L_{13} = 0.251 \pm 0.0125$ nm, and $\sigma_{intra} = 0.276$ nm where L_{12} is the covalent bond distance, L_{13} is the bond distance for sites

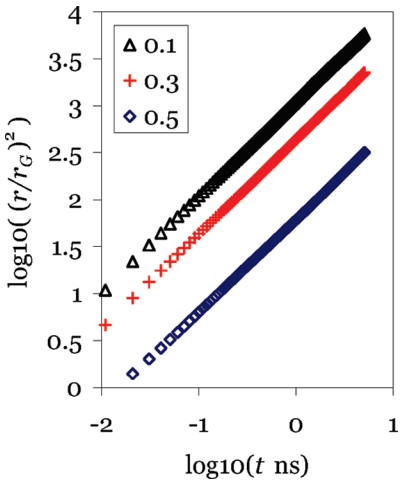

Figure 1. Mean squared displacement for the *n*-hexane reference fluid. For *n*-hexane, $\langle r_G \rangle = 0.21$ nm. Packing fractions are listed in the legend.

Table 1. Parameters Used for Each Site Type in *n*-Alkanes

	σ (nm)	M_w (g/mol)
CH_4	0.367	16.0428
CH_3-	0.363	15.0349
CH_2-	0.357	14.0269

Table 2. Database of the Self-Diffusivity for the *n*-Alkanes, Available as an Online Supplement

	T_c (K)	M_W	m^{Eff}	V^{Eff}	ref
methane	190.63	16.04	1.00	0.03	27, 29, 55, 56, 28
ethane	305.43	30.07	1.10	0.04	29, 55
propane	369.82	44.1	1.15	0.06	29, 57
n-butane	425.16	58.12	1.25	0.07	58, 59
n-hexane	507.3	86.18	1.51	0.10	60, 61, 55, 62
n-heptane	540.2	100.20	1.68	0.11	63, 60
n-octane	568.69	114.23	1.81	0.13	60, 64, 62
n-nonane	594.6	128.25	1.94	0.14	63
n-decane	617.55	142.29	2.10	0.16	60, 63, 64, 62
n-dodecane	658	170.34	2.43	0.18	63, 62
n-hexadecane	725	226.45	2.99	0.24	30

separated by two bonds (defining bond angle), and σ_{intra} is the intramolecular repulsive diameter for sites separated by 3−7 bonds (defining dihedral angle distribution). The intramolecular diameter for sites separated by more than seven bonds is the same as the intermolecular diameter.

The self-diffusivity was computed for chain lengths up to $N_c = 117$ at 300 K and packing fractions ranging from 0.1 to 0.5, where N_c is the carbon number. Table 2 summarizes the diffusivity results for each chain length. Sample results are illustrated in Figure 1. Figure 1a presents the diffusivity in terms of ρD, where D is the diffusivity in cm^2/s and ρ is the ***mass*** density (g/cm^3). We apply the mass density here because we are interested in scaling with regard to polymer liquids, as well as Enskog gases. The number density, typical for Enskog gases, is not useful for polymers. While scaling studies of polymer liquids focus primarily on the diffusivity alone, the diffusivity alone diverges at low density. Duly noting that scaling in polymer liquids is generally considered at constant pressure, rather than constant density, we prefer to study a quantity that is always finite. Variations in polymer density with molecular weight tend to be relatively small, so we do not expect qualitative deviations from the analysis based on mass density.

A striking feature of Figure 1a is that the diffusivity of small molecules is actually smaller than that of large molecules at the same mass density when the density is high. This peculiarity is a consequence of two effects: (1) the molecular density of the monomer is low relative to that of a fused sphere chain, making the mass density low even at high packing fractions. (2) The small molecules approach their glass transition packing fractions (η_g) at lower densities than the large molecules.

The next important feature of Figure 1a is the manner in which the diffusivity in the low-density limit varies with molecular weight. This trend in the intercepts is illustrated in Figure 1b, where we extrapolated the simulation data to zero by fitting to the equations discussed below. Understanding this trend in the low-density limit requires further detailed analysis.

The usual starting point for diffusivity is to characterize D_o where D_o is the diffusivity in the hard sphere, low-density limit. D_o is determined by the Enskog relation:

$$\rho D_o = \frac{3M}{8N_A\sigma^2}\left(\frac{RT}{\pi M}\right)^{1/2} \tag{2}$$

where N_A is Avogadro's number, R is the gas constant, T is the absolute temperature in Kelvins, σ is the equivalent hard sphere diameter. Difficulties arise when attempting to characterize σ for a chain molecule. Salim and Trebble assumed that $\sigma_C^3 = m^{Eff} \times \sigma_{mon}^3$ and $M_C = m^{Eff} \times M_{mon}$ where m^{Eff} is the effective number of tangent sphere segments.[19] We refer to this as the volume conservation assumption. Yu and Gao[3] showed that this assumption leads to

$$\rho D_o^C = \frac{3M}{8N_A(m^{eff})^{2/3}\sigma_{mon}^2}\left(\frac{RT}{\pi m^{eff} M_{mon}}\right)^{1/2} = \frac{\rho D_o^{mon}}{(m^{eff})^{1/6}} \tag{3}$$

where

$$\rho D_o^{mon} = \frac{3M_{mon}}{8N_A\sigma_{mon}^2}\left(\frac{RT}{\pi M_{mon}}\right)^{1/2} \tag{2}$$

M_{mon} is the molecular weight of the reference monomer, and σ_{mon}(nm) is the diameter of the reference monomer. By assuming $M_{mon} = 0.016034$ kg/mol, $\sigma_{mon} = 0.36$ nm, similar to methane, we obtain $\rho D_o^{mon} = 0.000171$ g/cm·s as a reference point for *n*-alkanes at 300 K. Since ρD_o^{mon} is a constant for a particular oligomeric series, its value does not affect the scaling with molecular weight. Equation 3 suggests that the low-density intercept should vary weakly with chain length, that is, to the $^1/_6$th power. The behavior in Figure 1b would seem to indicate a stronger variation than that.

Regression of the trends for each chain can be used to achieve a more quantitative analysis of the scaling in the low-density limit. The analytical formula for hard spheres developed by Sigurgeirsson and Heyes[18] has been adapted for fused hard sphere chains. This correlation can be modified for chains as follows:

$$\frac{\rho D_C}{\rho D_o^{mon}} = \left(1 - \frac{\eta}{\eta_g}\right)\left(1 + d_2(m^{Eff})\left(\frac{\eta}{\eta_g}\right)^2 - d_4(m^{Eff})\left(\frac{\eta}{\eta_g}\right)^4\right)C(m^{Eff}) \tag{4}$$

$$\eta_g = 0.57 + 0.43(m^{Eff} - 1)/m^{Eff} \tag{5}$$

The trend for η_g, eq 5, was determined by matching the values for spheres from Sigurgeirsson and Heyes and the value of 1.0 in the long chain limit. More precise characterization of η_g did not affect the accuracy of the correlations and it was helpful to reduce the number of parameters in the model. The parameters in eq 4 can be correlated for fused hard sphere chains as:

$$d_i = d_i^{HS} - d_i^{FS}\left[\frac{(m^{Eff} - 1)}{m^{Eff}}\right] \quad (6)$$

where $d_2^{HS} = 0.4740$ and $d_4^{HS} = 1.1657$ are taken from the work of Sigurgeirsson and Heyes. Values of d_2^{FS} and d_4^{FS} are derived from regression of the FS chain simulation results. The data Figure 2b were obtained by treating d_2, d_4, and ρD_o as adjustable parameters specific to each component.

In eq 4, $C(m^{Eff})$ is introduced to address the scaling in the long chain limit, where eq 6 approaches an asymptotic value. For long chains, scaling of the self-diffusivity is widely held to follow either the Rouse model or the reptation model.[20] Tao et al.[21] briefly summarize the state of the art as

$$\frac{kT}{D_{Rouse}} = \frac{M}{M_{mon}} f(T, \rho, ...); \quad \frac{D_{reptation}}{D_{Rouse}} = \frac{M_e}{M} \quad (7)$$

where M is the molecular weight, M_e is the molecular weight at which entanglement effects become significant and may vary substantially depending on the molecular structure. Below M_e, molecules behave more like oligomers than true polymers; f is a phenomenological "monomeric" friction parameter that may depend on the temperature, density, and molecular architecture. We also assume that f may be a relatively weak function of chain length for very short chains. In this sense, f is regarded as more phenomenological than monomeric. Experimental data on diffusivity scaling are often difficult to interpret because the density varies with the molecular weight and temperature in experiments where the pressure is held constant. When plotting diffusivity versus molecular weight, apparent scaling can vary from $M^{-1.85}$ to $M^{-2.72}$. Nevertheless, careful interpretation leads to the form of eq 7 in the final analysis.[22] While we do observe transitions in scaling that are indicative of entanglement during our molecular simulations, the primary focus of the present work is below M_e. Thus we seek a function scaling as M^{-1} in the long chain limit. Noting that the simulated temperature is constant for the hard FS chains of the reference system, and density effects are accounted for by d_i^{FS}, we obtain the following for FS chains.

$$m^{Eff} C(m^{Eff}) = 1 + c_1\left(\frac{m^{Eff} - 1}{m^{Eff}}\right) + c_2\left(\frac{m^{Eff} - 1}{m^{Eff}}\right)^2 \quad (8)$$

With $c_1^{FS} = 1.662$, $c_2^{FS} = -1.005$, $d_2^{FS} = 3.733$, and $d_4^{FS} = 2.619$, FS chain simulation results were correlated to 5.5% average absolute deviation (%AAD). The curve shown in Figure 2b was obtained from the eq 8 with the values of c_1^{FS} and c_2^{FS} optimized for all components over all densities. This curve indicates that eq 8 provides a satisfactory description of the trend, including the scaling for large m^{eff}. As another way of representing this scaling, one could write that $\sigma = \sigma_{mon}{}^{0.75}$. The curvature in Figure 2b means that the impact of chain length is small for chains smaller than *n*-hexane, possibly leading to confusion about the viability of the equivalent hard sphere perspective. The reason for this curvature is that the CH_3 diameter is larger than the CH_2 diameter.

3. Temperature Effects

Having established the methodology of self-diffusivity calculations for hard FS chains, the SPEADMD model must be generalized to correlate experimentally observed self-diffusivities of compounds including *n*-alkanes, branches, rings, and heteroatoms. Naturally, the effects of attractive forces must be taken into account. Furthermore, contrary to previous findings for the thermodynamic properties, accounting for effects of the softness of the intermolecular interactions was found to be necessary. The softness was a relatively small effect and is addressed first. Effects of attractive forces are substantial, as discussed in the subsequent subsection. The primary database consists of C1−C16 *n*-alkanes, for which diffusivities and densities are known over a fairly wide range of temperatures and pressures. These data are supplemented with the ambient pressure data of von Meerwall et al. for C8−C60 over a temperature range of 30−170 °C. A summary of the database including literature sources is given in Table 2. In some cases, authors did not report the densities corresponding to the experimental self-diffusivities. For C1−C16, the REFPROP computer program[23] was used to calculate densities. For C20−C60, the density correlation of von Meerwall et al. was applied.

3.1. Correction for the Softness of *n*-Alkanes. Preliminary application of eq 4 to the *n*-alkane database showed that the diffusivities of small molecules tended to be systematically underestimated. The nature of this behavior is illustrated for methane by the dashed curve in Figure 3. Note that the magnitude of the discrepancy becomes larger as the temperature increases. The observations that the discrepancies are largest for small molecules at high temperature suggest that the discrepancy results from the softness of the potential. Large molecules are less susceptible to this influence because the interior atoms tend to overlap substantially, generating an effectively harder core. High temperatures exaggerate the effect because the higher kinetic energy enables greater penetration of the soft core. The solid curve in Figure 3 presents results after correcting for the softness of the potential.

Treating the sphere diameter as being temperature-dependent permits correction for softness. A simple correlation for the temperature dependence of the equivalent hard sphere diameter of the LJ potential has been presented by Elliott and Daubert.[24]

$$\frac{d^{EHS}}{\sigma} = 2^{1/6}(0.6288(T^*)^2 + 11T^* + 1)^{-1/25} \quad (9)$$

where d^{EHS} is the equivalent hard sphere diameter based on the Barker−Henderson[25] formula applied to the Weeks−Chandler−Andersen[26] characterization of the LJ potential, and $T^*(= k_B T/\varepsilon^{LJ})$ is a reduced temperature. We correlate $\varepsilon^{LJ}/k_B = 79$ K as the reference energy for all softness corrections. Since the softness is apparent primarily for the sites at chain ends, this correction is applied only to one effective carbon atom per molecule. The result is a reduction in the estimated molecular volume, consequently reducing the effective packing fraction at a given mass density.

$$\frac{V^{soft}(T)}{V^{Eff}} = 1 - \frac{\pi}{6}\frac{\sigma_{mon}{}^3}{V^{Eff}}\left[1 - \left(\frac{d^{EHS}}{\sigma}\right)^3\right] \quad (10)$$

where V^{Eff} is obtained from the simulation results based on the hard reference potential, and for *n*-alkanes, $\sigma_{mon} = 0.36$ nm as defined in eq 3.

An additional effect of softness arises in defining the diffusivity of the reference monomer, $\rho D_o{}^{mon}$. If the reference monomer were maintained as a hard sphere, then the diffusivity of methane would approach that of the hard sphere even at high temperatures and low densities, where the effective hard sphere diameter should have shrunk. On the other hand, the reference monomer should not shrink substantially for long chains, because the cooperative repulsion in a fused-sphere chain resists shrinkage except at the chain ends. We can achieve a balance

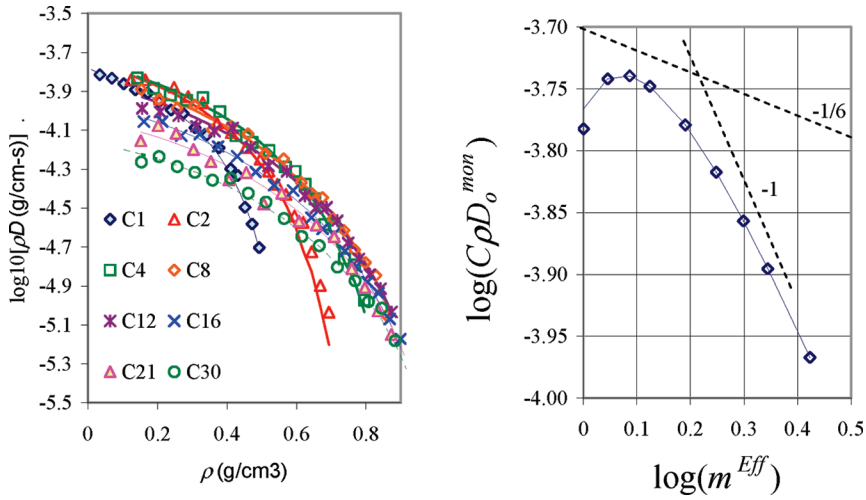

Figure 2. Simulated diffusivities of FS chains. (a) In terms of mass density showing how small chains have lower diffusivities than large ones at high density. (b) In terms of packing fraction, showing simpler scaling with molecular size. Data points are simulation results and solid lines based on eq 4.

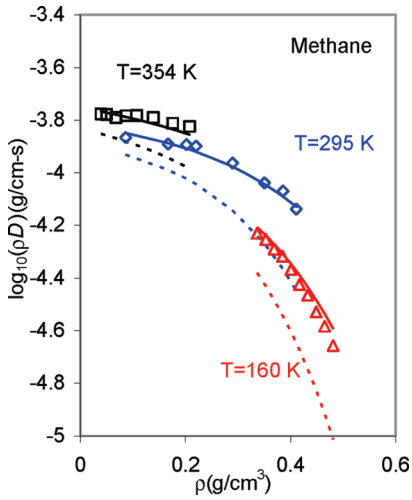

Figure 3. The self-diffusivity results of methane. Dashed lines represent eq 4 based on purely repulsive potential simulations. Solid lines show results after introducing the softness correction of eq 10. Points represent data of refs 27−29.

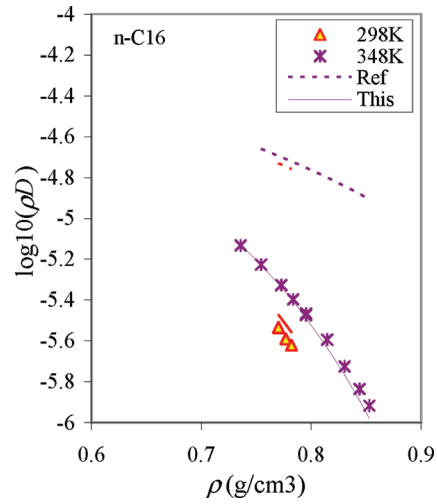

Figure 4. The self-diffusivity of *n*-hexadecane ($C_{16}H_{34}$) at atmospheric pressure and $T = 298-443$ K. Dashed lines represent correlation based on purely repulsive model (eqs 4 and 10 combined). Solid lines include the attractive correction (eq 16). Data points are taken from refs 30 and 22.

between these perspectives by recognizing that the low-density reference pertains to the limiting value for the entire chain, not just the monomer, making it most appropriate to focus on the quantity $\rho D_o^{mon} C$. Noting the temperature dependence of $\rho D_o^{mon} C$, we write for *n*-alkanes:

$$\rho D_o^{mon} C = 0.000171 C \left(\frac{V^{Eff}}{V^{soft}}\right)^{2/3} \left(\frac{T}{300}\right)^{1/2} \qquad (11)$$

where we have also included the temperature correction for the molecular velocity. Even though the factor C cancels in eq 11, we write it in this way to emphasize that the long chain is less affected by softening than the monomer alone. This helps to clarify that the correction should be $(V^{Eff}/V^{soft})^{2/3}$, as for a chain, rather than $(\sigma/d^{ehs})^2$ as for the monomer alone.

3.2. Corrections for Attractive Forces. The importance of attractive effects for longer chains is illustrated in Figure 4. Equation 4 overestimates the diffusivity for long chains. To correct for this discrepancy, the effect of attractive forces needs to be incorporated.

Observations of the attractive effects on diffusivity have been studied in some detail for spherical molecular models. Speedy et al.[31] reviewed computer simulation data for the square-well and Lennard-Jones models. Meier et al.[32] performed extensive simulations of the transport properties of the Lennard-Jones model over wide ranges of temperature and density. Furthermore, hydrogen bonding reduces the self-diffusivity as shown by Liu and Elliott.[33] Figure 5 illustrates that the addition of a square-well to hard spheres lowers the diffusivity at all densities.[34] Unfortunately, the results for the LJ potential are difficult to interpret because the softness of the potential is coupled with the attractive effect.

Recently, Theodorou and co-workers[7] presented results from 300 ns atomistic molecular dynamics simulations of polyethylene melts, ranging in molecular length from C78 to C250. Similar to the SPEADMD model, a fused-sphere, united-atom description was used in their work. Nonbonded interactions were described by a Lennard-Jones potential. Their MD simulations have been conducted in the canonical (*NVT*) ensemble, at $T =$ 450 K with densities selected such that $P \approx 1$ bar. Initial configurations were obtained from end-bridging Monte Carlo simulations and densities at the same T and ρ equal to 0.775, 0.790, 0.795, 0.8, and 0.8 g/cm^3 for the C78, C156, C180, C200, and C250 PE melts, respectively. To provide an evaluation of the attractive effects in long chains, we simulated similar melts at similar conditions using the SPEADMD repulsive model. In

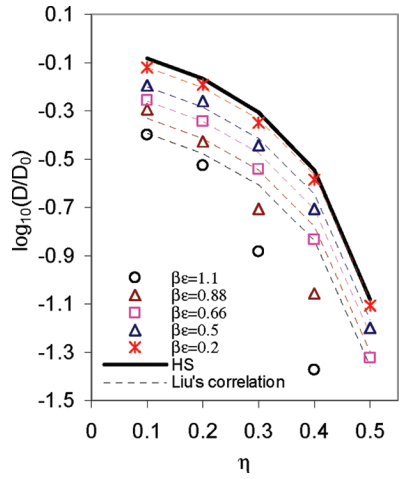

Figure 5. Reduced self-diffusivity obtained from SW potential models at $T_r \approx 1-4$. Points indicate MD data for a square-well fluid[34] and curves represent the LHV theory (eq 12).

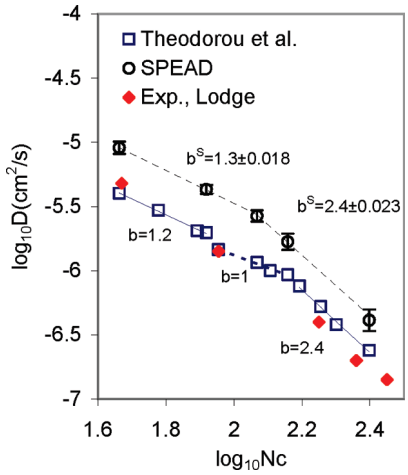

Figure 6. Predicted and experimental (ref 21) self-diffusivity D vs chain length N_c ($T = 450$ K; $P = 1$ bar in Harmandaris et al.). Harmandaris et al. include attractive effects while SPEADMD is just for the reference system and at constant density.

contrast to the situation for LJ spheres, the softness of the potential plays an insignificant role for these longer chains. Initial configurations were obtained at $T = 450$ K and $\eta = 0.5$, with corresponding densities, ρ, equal to 0.82, 0.82, 0.83, and 0.83 g/cm^3 for the C_{46}, C_{83}, C_{117}, and C_{250} molecules, respectively. Each simulation consisted of 32 independent chains. Simulated time was 20 ns in each case with 10 ps updates. These simulations required roughly 21, 52, 89, and 293 h. Our simulations are shorter than Theodorou's work because these initial simulations are aimed at qualitatively exploring the attractive effect in the crossover regime. Figure 6 presents the comparison, also including the experimental data of Tao et al.[21]

As expected from the neglect of attractive effects, SPEADMD simulated diffusivities are higher than both experimental data and the atomistic MD results of Harmandaris et al.[7] Nevertheless, the magnitude of the attractive effect is consistent even through the entanglement transition. This indicates that the attractive effect for long chains acts like a uniform background correction, the magnitude of which approaches an asymptotic value at high molecular weight. In this sense, the attractive friction differs from the repulsive friction because the repulsive friction is proportional to molecular weight for long chains. Furthermore, the purely repulsive model of SPEADMD captures the phenomenology of the entanglement transition, lending further support to the basic concept of using rigorous reference simulations to establish the phenomenology.

Developing a quantitative correlation for diffusivity requires the assumption of a functional form for the attractive correction. On the basis of our experience with TPT, it is natural to seek a perturbation expansion for the effects of attractive forces on diffusivity. Unfortunately, Alder et al. have argued that a logarithmic singularity exists in the high temperature, low density limit of the inverse temperature expansion, suggesting that such a perturbation expansion may not formally exist.[35] On the other hand, Longuet-Higgins and Valleau (LHV) developed an analytical theory for the effect of attractive forces on the diffusivity of square-well spheres and Davis, Rice, and Sengers (DRS) extended this approach to viscosity and thermal conductivity.[36,37] Their approach focused on explicit treatment of each type of collision instead of lumping all contributions into factors of inverse temperature, and included the assumption that the various collision types were uncorrelated. Note that, the original LHV work includes a modified Bessel function of the second kind (K_1), giving a similar kind of nonanalytic behavior to that observed by Alder et al. in the high temperature expansion. Karkheck et al. emphasized that the singularity observed by Alder et al. exists in terms of order $\ln(T)/T^2$ and higher, not the first order term. Furthermore, the first order term turns out to be "unreasonably accurate,"[38] suggesting that some form of renormalization may be required to cancel the singularity. On the other hand, Davis and Luks presented an alternative formulation of the attractive correction that seems to eliminate the singularity by replacing K_1 with the analytic integral formula below.[39] The LHV result then becomes

$$\frac{D_0^{HS}}{D^{SW}} = g(\sigma) + \lambda^2 g(\lambda\sigma)\Xi \tag{12}$$

$$\Xi = \exp(\beta\varepsilon) - 0.5\beta\varepsilon - 2\int_0^\infty x^2(x^2 + \beta\varepsilon)^{1/2}\exp(-x^2)\,dx \tag{13}$$

where $\beta = 1/k_BT$ and λ is the square-well width.

Empirically, observing the trends in temperature for square-well spheres also suggests that a perturbation approach should provide an accurate correlation, and Alder et al.[35] have suggested extracting the expansion coefficients by fitting simulation results, though they have warned against assuming a particular functional form. Dufty et al. emphasized that the LHV/DRS assumption of uncorrelated (partial) collisions is questionable at low density.[40] They further noted that the completed collision theory of Hofmann and Curtis[41] solves this problem at low density but fails at moderate to high densities. They concluded that further progress must focus on carefully explaining the transition from partial to completed collisions. Altogether, this background leaves rigorous transport theory suggesting an expansion, but not committing to a particular functional form.

To make progress, we assume that the relation between the diffusivity and the friction coefficient can be expressed as

$$\ln\left(\frac{D_o^{mon}}{D}\right) = \ln(f^R) + \frac{\Lambda(\eta, m^{eff})}{T} \tag{14}$$

where f^R is the friction coefficient due to the reference potential and Λ represents the perturbation coefficient for attractive effects. f^R and Λ are defined as

$$f^R = \left(\frac{\rho D_o^{mon}}{\rho D^{ref}}\right) \tag{15}$$

$$\Lambda = \eta_r^2 \varepsilon/k_B \tag{16}$$

where $\eta_r \equiv \eta/(1 - \eta/\eta_g)$ and ρD^{ref} is the contribution of the reference fluid obtained from eqs 4 and 10. The form of eq 14 makes it clear that diffusivity decreases as friction increases. The form of eq 16 reflects our conjecture that the integral of eq 13 is indeed analytic. This gives a relation for diffusivity that is similar to TPT which says

$$\left(\frac{A - A^{ig}}{RT}\right) = A^R + \frac{A_1(\eta)}{T} + \frac{A_2(\eta)}{T^2} \tag{17}$$

Hence the same perspective is adopted for both diffusivity and free energy. Specifically, the reference fluid is expected to dominate the qualitative features of the behavior and the attractive field to act as a perturbation. In all cases, the reference contribution is to be computed by simulation, giving rigor to the most important feature of the model. Noting the lack of a rigorous perturbation theory for transport properties, we feel justified applying an empirical approach to their characterization at this time. ε/k_B is estimated from

$$\varepsilon/k_B = 0.6T_c(e_0 + e_1\Delta + e_2\Delta^2) \tag{18}$$

The remaining parameters are obtained by minimizing the root-mean-square of deviations of methane through *n*-hexadecane between experimental data and eq 14. The values of regressed parameters for spherical molecules are $e_0 = 0$, $e_1 = 0.56$, $e_2 = 1.26$. Overall, 8.6% AAD with −0.4% bias is obtained for 657 data points from ethane through *n*-hexadecane. The entire database is available online as supplemental data associated with this publication. Typical results are illustrated for *n*-hexadecane in Figure 4. Note that the value of $e_0 = 0$ implies that we ignore attractive effects in methane. Over the range of the available data, the attractive friction for methane is roughly canceled by the repulsive softening, resulting in reasonable accuracy (10.0% AAD). While this is clearly an oversimplification, our primary interest is in a generalized correlation for nonspherical molecules. Therefore, we judge this anomaly to be acceptable for the present analysis.

In closing, it is valuable to consider the implication of the logarithmic form of eq 14. We initially tried a polynomial form for adding attractive effects, but found that accuracy and trends were unsatisfactory, despite the inclusion of nine adjustable parameters, compared to four in the present correlation. Referring again to Figure 4, the slope of the repulsive curve is too weakly density dependent compared to the experimental trend. Therefore, the attractive correction must multiply the repulsive contribution rather than simply providing an additive shift. Physically, we interpret this to mean that the attractive forces amplify the repulsive friction rather than simply adding to it.

4. Comparisons to Existing Correlations

The measured diffusivity, *D*, of a real liquid is most often correlated by[42]

$$D = CD_{HS} \tag{19}$$

where $D_{HS}(T, n, \sigma)$ is a function of the temperature *T*, the number density *n*, and the effective hard sphere diameter σ, and $C(T, \rho)$ is a correction factor that accommodates any influence on *D* of effects that are not present in the purely repulsive potential model. Questions then arise as to whether σ and *C* are temperature and/or density dependent parameters. The answers to those questions are often contradictory. Chandler's rough hard sphere (RHS) theory[43] uses the hard sphere as a reference system and diffusivity is written as $D \approx D_{RHS} = AD_{HS}$ where *A* is a translational−rotational coupling factor that accounts for the nonsphericity of the molecule. The coupling factor may depend on both temperature and density,[44] but for nonspherical fluids, no equation is available for this factor. Moreover, it has been recognized that the coupling factor introduced as a perturbation to the hard sphere reference system is found (on fitting the equations to the experimental data) to be strongly temperature dependent.[29,45] Another approach is based on the Weeks−Chandler−Andersen (WCA)[26] repulsive potential used as a reference system. Straub[46] found on the basis of MD simulations that D_{LJ} can be expressed with D_{WCA} and corrected by $(1 + \alpha(\beta\varepsilon))$ where α is a constant. D_{WCA} is calculated using the expression for a hard sphere fluid in which the molecular diameter is replaced by effective hard-sphere diameter. Many empirical correlations primarily correlate the effective hard sphere diameter with temperature and density, and lump the effects of attractive forces into this repulsive parameter. Heyes and Branka[47] have recently questioned the usefulness of the effective hard-sphere concept. Liu and co-workers have developed a typical implementation of this approach.

In Liu's approach,[1] the self-diffusivities are correlated with the equations for the HS, SW, and LJ fluids. Liu's correlation can be written as

$$D_{LJ}^{real} = \frac{21.16}{\rho(\sigma_{eff}^{BMD})^2}\sqrt{\frac{1000RT}{MW}}x \exp\left\{-\frac{0.75(\sigma_{eff}^{BMD})^3}{1.2588 - \rho(\sigma_{eff}^{BMD})^3} - \frac{0.27862(\varepsilon_{LJ}/k)}{T}\right\} \tag{20}$$

where ρ is number density, σ_{eff}^{BMD} is effective hard sphere diameter (EHSD), and this Boltzmann EHSD equation is obtained by fitting temperature to the MD self-diffusivities for the repulsive LJ fluid and is defined as

$$\sigma_{eff}^{BMD} = \sigma_{LJ}2^{1/6}\left[1 + \sqrt{\frac{1.3229T}{(\varepsilon_{LJ}/k)}}\right]^{-1/6} \tag{21}$$

Liu's correlation provides excellent accuracy when both σ_{LJ} and ε_{LJ} are treated as adjustable parameters, but there is no trend in the parameters that can be used to predict diffusivities for unknown compounds.

A corresponding states method has been proposed by Zabaloy et al.[2] based on the LJ fluid. The parameters were obtained by fitting the molecular simulation data of Meier et al.[32] to a multiparameter equation of state in terms of the temperature and density or pressure. The LJ parameters σ and ε are the most important parameters in this correlation. They use a corresponding states approach to define diameter and attractive strength in terms of thermodynamical data.

In another method proposed by Yu and Gao,[3,48] the diffusivity of a polyatomic fluid is represented as the sum of three friction coefficients: the temperature-dependent hard-sphere correlation, the chain contribution, and the soft contribution. This method is similar to the present work in using MD simulation results to characterize the hard-sphere and chain contributions. They base their correlation on the TS chain results of Smith et al. however, whereas the present method applies the diffusivity from the SPEADMD molecular model directly. The Yu−Gao method is similar to Liu's approach in that the segment diameter σ_{LJ}, segment−segment interaction energy ε_{LJ}, and the number of segments m^{Eff} are

Table 3. Corrected Simulation Results of Straight Alkane Chains Are Fitted into eq 14 and Compared to Modified Version of Empirical Correlation by Liu et al.[1] in the Literature

	NDP	σ_{Eff} (nm)	ε/k_B (K)	T_{min} (K)	T_{max}(K)	P_{min} (MPa)	P_{max} (MPa)	ρ_{min} (g/cm^3)	ρ_{max} (g/cm^3)	SPEADMD % AAD	SPEADMD % bias	Liu/Silva % AAD	Liu/Silva % bias
CH_4	296	0.367	114.34	110	454	0.8	221.6	0.008	0.528	10.0	7.5	6.55	3.54
C_2H_6	71	0.415	183.26	136	454	25.0	200.0	0.238	0.672	14.7	–14.6	21.39	–21.39
C_3H_8	55	0.452	221.89	112	453	0.1	200.0	0.370	0.756	13.4	3.5	27.86	–26.14
C_4H_{10}	18	0.475	255.10	177	451	0.1	200.0	0.518	0.741	17.4	–1.4	22.53	–14.30
C_6H_{12}	63	0.498	304.38	223	333	0.1	393.8	0.614	0.819	6.2	–2.2	5.54	3.76
C_7H_{16}	27	0.504	324.12	173	373	0.1	0.1	0.613	0.778	3.9	–1.1	8.90	5.77
C_8H_{18}	50	0.512	341.21	248	348	0.1	360.8	0.658	0.834	3.6	–1.0	24.42	24.42
C_9H_{20}	12	0.519	356.76	236	423	0.1	0.1	0.609	0.764	2.7	0.2	28.96	28.96
$C_{10}H_{22}$	24	0.521	370.53	250	440	0.1	60.0	0.610	0.763	7.1	0.1	44.60	44.60
$C_{12}H_{26}$	16	0.526	394.92	263	433	0.1	60.0	0.644	0.787	7.6	1.3	73.32	73.32
$C_{16}H_{34}$	25	0.537	432.36	298	348	0.1	279.2	0.736	0.853	8.0	3.5	163.26	163.26
all	657									8.6	–0.4	38.85	25.98

Table 4. Corrected Simulation Results of Straight Alkane Chains Are Fitted into eq 14 and Compared to Available Empirical Correlation Based on Molecular Simulation Results by Zabaloy et al.[2]

	T_{min} (K)	T_{max} (K)	P_{min} (MPa)	P_{max} (MPa)	Zabaloy et al. NDP	Zabaloy et al. σ_{Eff} (nm)	Zabaloy et al. ε/k_B (K)	Zabaloy et al. % AAD	Zabaloy et al. % bias
methane	110	454	0.8	221.6	296	0.391	142.25	19.4	–2.57
ethane	136	454	25	200	56	0.449	228.001	43.31	26.65
propane	112	453	0.1	200	46	0.501	276.07	64.45	60.17
n-butane	177	451	0.1	200	16	0.545	317.38	104.19	93.42

regressed from the experimental diffusion data on a compound-specific basis.

Table 3 provides quantitative model performance information for *n*-alkanes and shows the number of experimental self-diffusivity data points (NDP) used for the fitting process, molecular diameter values, attractive well strength ($\varepsilon/k_B = 0.6\ T_c$), maximum and minimum temperature and pressure values, average absolute average deviation (AAD%) and bias% values. The root mean squared error (RMSE) deviation is defined as

$$\mathrm{RMSE} = \sqrt{\frac{1}{\mathrm{NDP}}\sum_{i=1}^{\mathrm{NDP}}\left[100 \times \frac{(D_i^{\mathrm{cal}} - D_i^{\mathrm{exp}})}{D_i^{\mathrm{exp}}}\right]^2}$$

The Liu correlation gives 7.2% AAD error when applied to our database for *n*-alkane chains using their optimized values for both parameters. In follow-up work,[1] Liu and co-workers showed that the correlation of self-diffusivity is more sensitive to diameter than to energy, such that the energy could be estimated from $\varepsilon/k_B = 0.774T_c$. The last two columns in Table 3 present the %AAD values obtained from this latter method, where we have optimized one parameter per compound. It appears that the Silva guideline for ε/k_B breaks down at higher molecular weights, emphasizing the empirical nature of Liu's correlation method. Overall, Liu's correlation can be used to correlate self-diffusivities, although the chosen set of ε/k_B and σ may have little relation to molecular properties, making them difficult to generalize.

A preliminary evaluation of the corresponding states method developed by Zabaloy et al. is shown in Table 4. This comparison shows that %AAD increases substantially as one progresses from methane to butane and presumably would continue to increase at higher molecular weights. Inconsistencies were observed during implementation so we did not perform an extensive analysis. These inconsistencies apparently occur from using the accurate density estimates obtained from REFPROP[23] instead of using a Lennard-Jones equation of state (EOS) developed by Kolafa and Nezbeda[49] as applied in the original correlation. Moreover, their model predicts negative diffusivity when it is applied to data at low

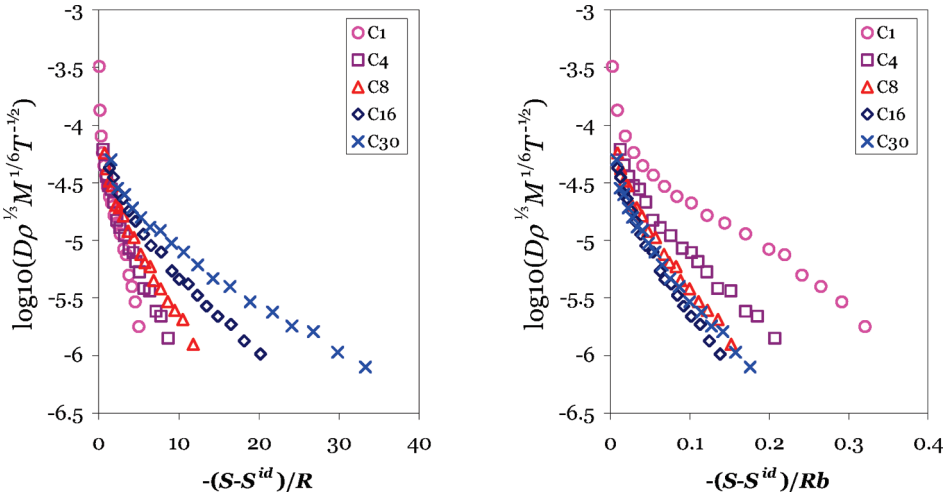

Figure 7. Evaluation of Rosenfeld's conjecture on the relation between diffusivity and entropy: (a) diffusivity vs entropy departure; (b) diffusivity vs entropy density. Note that ρ is the mass density here. In Rosenfeld's notation, ρ was the number density.

Table 5. Database of the Self-Diffusivity for Non-alkanes Available as Online Supplement

compound	M_W	T_c (K)	m^{eff}	$C\rho D_o^{ref}$	% AAD^{ref}	ref
argon	39.95	150.86	1.000	–3.549	4.4%	65, 66
hydrogen	2.02	33.27	1.048	–3.722	7.1%	67
CS_2	76.13	552	1.075	–3.673	13.8%	68
CO_2	44.01	304.2	1.114	–3.575	18.0%	69, 57
ethylene	28.05	282.41	1.200	–3.727	3.5%	70, 71
cyclohexane	84.16	553.54	1.081	–3.787	14.1%	54
benzene	78.11	562.05	1.175	–3.704	4.8%	53, 60, 72, 73
toluene	92.14	591.79	1.240	–3.779	5.6%	64
chlorobenzene	112.56	632.39	1.138	–3.656	4.7%	63
CH_3Cl	50.49	416.25	1.143	–3.614	5.0%	63, 74
CH_2Cl_2	84.93	510	1.129	–3.589	4.8%	74
$CHCl_3$	119.38	536.4	1.163	–3.666	4.8%	60, 75, 74
CF_3Cl	153.82	556.35	1.147	–3.620	4.0%	76, 60, 72
CCl_4	70.01	299.3	0.975	–3.656	7.1%	77
CHF_3	104.46	302	1.086	–3.595	6.2%	56
CF_4	88.00	227.5	1.157	–3.588	3.2%	78
SF_6	146.06	318.69	0.950	–3.630	9.4%	79, 80
$cycloC_4F_8$	200.03	388.37	0.950	–3.804	12.3%	81
ammonia	17.03	405.65	1.000	–3.698	3.6%	60, 82
acetone	58.08	508.2	1.217	–3.750	4.6%	60, 63
pyridine	79.10	619.95	1.302	–3.698	5.4%	83
methanol	32.04	512.6	1.152	–3.647	3.6%	60, 84, 59
ethanol	48.07	513.92	1.219	–3.656	3.7%	60, 84, 59, 45
water	18.02	647.1	1.000	–3.497	6.0%	60, 85–87

temperatures (e.g., $T = 136$ K). Therefore, this model must be limited to specific temperature and pressure ranges.

Overall, our proposed correlation works quite well over a wider range of conditions than available correlations. The appendix provides a sample calculation for methane and *n*C16 that illustrates how the Elliott−Gray trends for the equation of state combine with eq 14 to obtain predictions of *n*-alkane diffusivity at any conditions of temperature, pressure, or density.

5. Evaluating Conjectures on the Relation between Entropy and Diffusivity

Rosenfeld has suggested a relationship between the self-diffusivity and the entropy departure function $\Delta s = (S - S^{id})/R$.[50] The suggested correlation is

$$\rho^{1/3}M^{1/6}D/T^{1/2} \approx B\exp(A^*\Delta s)$$

This relationship is largely empirical, but it has been investigated by Mittal et al.[51] They found that the correlation was quite accurate for hard spheres and Lennard-Jones spheres, but less so for square well spheres. If successful, such a correlation would provide a valuable link between thermodynamic properties and transport properties.

Similar to the generalized correlation for diffusivity of any chain length, Elliott and Gray have characterized the terms of TPT for *n*-alkane chains.[52] Combined, these results provide a basis for evaluating Rosenfeld's conjecture. In particular, the entropy departures for hard chain fluids (given by *A*0) can be compared to their simulated self-diffusivities. The trends of the self-diffusivity versus entropy can thus be evaluated for the reference fluids.

Figure 7 shows that Rosenfeld's conjecture is not directly applicable to reference chain fluids. The characterization of the entropy in each case is the departure from the ideal chain entropy at zero density. Previous reports[51] have referred to this quantity as the "excess entropy," but we reserve the term "excess entropy" to refer to the deviation from ideal solution behavior in mixtures, a topic of a future report. To clarify, we compute the entropy departure from

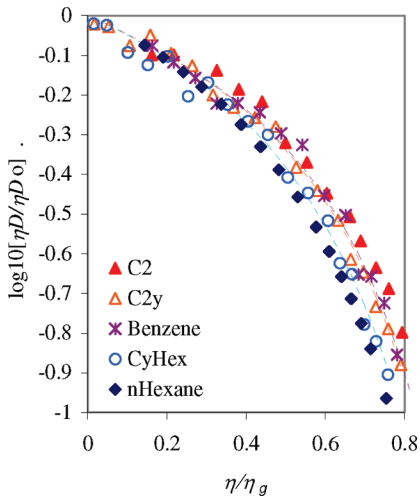

Figure 8. $D\eta$ normalized by the low density limit values $D_0\eta$ for ethane, hexane, benzene, cyclohexane, and ethylene. The dashed lines correspond to model predictions based on the repulsive potential by optimizing effective segment number equivalent to alkane results.

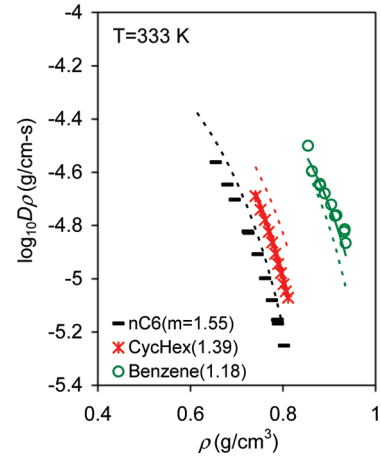

Figure 9. Comparison of experimental data and model predictions of benzene and cyclohexane at 333 K. The data for hexane are for comparison. Solid lines correspond to model predictions based on attractive effect with optimized values for $\varepsilon/k_B = 220$ K for benzene, and $\varepsilon/k_B = 507$ K for cyclohexane. Dashed lines are predictions with $\varepsilon/k_B = 0.6T_c$. Points are experimental data: (○) benzene,[53] (∗) cyclohexane,[54] and (—) hexane.[55]

$$\left(\frac{A - A^{id}}{RT}\right) = \int_0^{\rho} \frac{Z - 1}{\rho}\, d\rho \tag{22}$$

Where $Z = PV/RT$. In the athermal limit, the internal energy departure $(U0-U0^{id})/RT = 0$, so

$$(A0 - A0^{id})/RT = (U0 - U0^{id})/RT - (S0 - S0^{id})/R = -(S0 - S0^{id})/R \tag{23}$$

The athermal limit eliminates ambiguities of softness in the intermolecular potential and its temperature dependence as well as the influences of attractive forces.

The ordinate in Figure 7 is based on the scaling suggested by Rosenfeld. The trend in Figure 7a generally converges at zero density, where all the chains tend to diverge because the scaling on density does not cancel the divergence in the diffusivity. At high density, however, the trends diverge strongly depending on chain length. In an attempt to correct for the effect of chain length, Figure 7b shows the trend when the entropy is divided by the van der Waals volume of the molecule, an entropy density. The molecular volume (cm^3/mol) was computed by sampling 200 conformations of each molecule over the course of the simulation. Figure 7b may indicate convergence to asymptotic behavior for long chains at high density, but the low density behavior is clearly separated in that case, owing in part to Rosenfeld's peculiar scaling with respect to density. While it may be possible to construct a correlation of diffusivity based on entropy, we find that the correlation based on packing fraction, as adapted from Sigurgiersson and Heyes, is physically reasonable and quantitatively satisfactory.

Table 6. Corrected Simulation Results (SPEAD-Corr) Fitted into eq 14 To Predict Self-Diffusivities of Various Compounds

	NDP	σ (nm)	ε/k_B (K)	T_{min}(K)	T_{max} (K)	P_{min} (MPa)	P_{max} (MPa)	ρ_{min} (g/cm^3)	ρ_{max} (g/cm^3)	m^{Eff}	AAD%	bias%
argon	39	0.340	126.28	308.15	322.55	0.72	41.55	0.011	0.597	1.00	11.56	–5.49
hydrogen	27	0.420	19.96	298.75	309.35	7.07	70.32	0.005	0.039	1.05	37.57	–37.57
CS_2	29	0.341	178.99	268.20	313.20	0.10	385.10	1.233	1.510	2.22	3.70	0.87
CO_2	65	0.350	337.97	273.15	348.15	1.03	49.85	0.017	1.085	1.48	49.21	–39.58
ethylene	92	0.398	164.28	123.15	398.15	2.04	272.17	0.061	0.686	1.10	18.32	–3.82
cyclohexane	39	0.484	447.10	313.00	383.00	0.10	214.00	0.699	0.833	1.51	3.30	–0.59
benzene	85	0.464	186.78	288.20	561.70	0.10	454.40	0.305	0.993	1.46	11.33	0.17
toluene	54	0.491	525.18	219.51	325.66	0.10	369.10	0.836	1.006	1.39	12.16	–4.63
chlorobenzene	15	0.463	217.88	229.36	408.16	0.10	0.10	0.980	1.168	1.70	9.73	–4.46
CH_3Cl	50	0.365	181.94	186.00	440.00	0.10	200.00	0.769	1.145	1.51	7.77	–0.64
CH_2Cl_2	25	0.359	181.47	186.00	406.00	0.10	100.00	1.106	1.559	2.08	14.11	5.47
$CHCl_3$	69	0.366	111.68	217.00	397.00	0.10	389.90	1.336	1.753	2.65	13.70	1.28
CF_3Cl	67	0.316	185.88	303.15	348.15	3.68	188.38	0.299	1.539	3.00	16.75	–8.90
CCl_4	32	0.335	296.79	283.20	333.20	0.10	147.50	1.517	1.730	3.86	37.22	–13.10
CHF_3[a]	21	0.337	136.04	142.00	246.00	10.00	100.00	1.267	1.646	2.10	31.77	–25.68
CF_4	54	0.314	118.59	243.15	348.15	2.47	44.99	0.114	1.340	2.63	15.19	–4.01
SF_6	44	0.373	305.97	240.00	398.00	0.63	182.70	0.088	1.850	2.04	9.07	–2.14
cycloC_4F_8	59	0.460	349.53	323.00	473.00	5.00	190.00	1.080	1.800	1.90	4.34	0.20
ammonia	27	0.316	166.26	196.90	297.84	0.10	0.10	0.602	0.733	1.19	8.34	–3.45
acetone	12	0.431	253.56	236.69	337.15	0.10	0.10	0.740	0.853	1.46	12.66	–6.09
pyridine[a]	47	0.462	407.21	303.15	423.15	0.10	500.00	0.862	1.106	1.45	10.62	–4.06
methanol	90	0.363	311.07	187.00	453.00	0.10	385.80	0.605	0.966	1.24	55.94	9.60
ethanol	74	0.414	747.37	263.00	437.00	0.10	265.20	0.637	0.921	1.24	41.36	–13.94
water	31	0.227	828.23	274.15	648.20	0.002	22.36	0.315	1.002	1.69	27.64	–14.84
overall	1147										19.29	

[a] Experimental data was close to η_g so the value of η_g was optimized: $\eta_g = 0.70$ for pyridine, and $\eta_g = 0.73$ for trifluoromethane.

Table 7. The Empirical Method Developed by Liu et al.[1] as Applied to Our Database Using Their Original Adjusted Parameters

	NDP	σ (nm)	ε/k_B (K)	T_{min} (K)	T_{max} (K)	P_{min} (MPa)	P_{max} (MPa)	ρ_{min} (g/cm^3)	ρ_{max} (g/cm^3)	AAD	bias %
argon	39	0.341	123.6	308.15	322.55	0.72	41.55	0.011	0.597	41.19	37.55
hydrogen	27	0.594	3.5×10^{-3}	298.75	309.35	7.07	70.32	0.005	0.039	96.54	–96.54
carbondisulfide	29	0.430	376.0	268.20	313.20	0.10	385.10	1.233	1.510	1.14	0.58
carbondioxide	65	0.326	500.7	273.15	348.15	1.03	49.85	0.017	1.085	8.47	4.22
ethylene	92	0.405	169.1	123.15	398.15	2.04	272.17	0.061	0.686	14.68	7.38
cyclohexane	39	0.573	224.9	313.00	383.00	0.10	214.00	0.699	0.833	2.32	0.35
benzene	85	0.519	308.4	288.20	561.70	0.10	454.40	0.305	0.993	5.47	2.62
toluene	54	0.545	350.7	219.51	325.66	0.10	369.10	0.836	1.006	56.61	–50.61
chlorobenzene	15	0.557	207.5	229.36	408.16	0.10	0.10	0.980	1.168	6.08	1.64
chloromethane	50	0.400	402.7	186.00	440.00	0.10	200.00	0.769	1.145	7.36	–3.24
dichloromethane	25	0.442	411.0	186.00	406.00	0.10	100.00	1.106	1.559	28.65	28.61
chloroform	69	0.476	505.3	217.00	397.00	0.10	389.90	1.336	1.753	11.05	–5.08
$CClF_3$	67	0.438	410.8	303.15	348.15	3.68	188.38	0.299	1.539	929.68	869.98
carbon tetrachloride	32	0.529	418.8	283.20	333.20	0.10	147.50	1.517	1.730	31.88	1.80
trifluoromethane	21	0.405	332.2	142.00	246.00	10.00	100.00	1.267	1.646	44.89	–44.89
carbontetrafluoride	54	0.433	244.0	243.15	348.15	2.47	44.99	0.114	1.340	7.29	0.46
sulfurhexafluoride	44	0.433	244.0	240.00	398.00	0.63	182.70	0.088	1.850	48.31	48.31
perfluorocyclobutane	59	0.620	71.0	323.00	473.00	5.00	190.00	1.080	1.800	3.83	0.07
ammonia	27	0.424	4.5	196.90	297.84	0.10	0.10	0.602	0.733	3.11	–0.65
acetone	12	0.467	333.0	236.69	337.15	0.10	0.10	0.740	0.853	77.87	77.87
pyridine	47	0.504	296.3	303.15	423.15	0.10	500.00	0.862	1.106	9.67	1.95
methanol	90	0.380	686.0	187.00	453.00	0.10	385.80	0.605	0.966	30.63	–18.50
ethanol	74	0.424	1291.4	263.00	437.00	0.10	265.20	0.637	0.921	86.71	–81.28
water	31	0.153	3788.5	274.15	648.20	0.002	22.36	0.315	1.002	23.79	–14.59
overall	1147									65.72	

Table 8. The Method Developed by Zabaloy et al.[2] as Applied to the Current Database

	NDP	σ (nm)	ε/k_B (K)	T_{min} (K)	T_{max} (K)	P_{min} (MPa)	P_{max} (MPa)	ρ_{min} (g/cm^3)	ρ_{max} (g/cm^3)	AAD	bias %
argon	39	0.355	112.62	308.15	322.55	0.72	41.55	0.011	0.597	10.14	2.22
hydrogen	27	0.332	24.836	298.75	309.35	7.07	70.32	0.005	0.039	640.07	640.07
CS_2	29	0.466	412.06	268.20	313.20	0.10	385.10	1.233	1.510	109.72	109.72
CO_2	65	0.391	227.08	273.15	348.15	1.03	49.85	0.017	1.085	13.39	9.27
ethylene	92	0.433	210.82	123.15	398.15	2.04	272.17	0.061	0.686	108.30	–33.70
cyclohexane	39	0.581	413.21	313.00	383.00	0.10	214.00	0.699	0.833	414.80	414.80
benzene	85	0.550	419.57	288.20	561.70	0.10	454.40	0.305	0.993	294.11	294.09
toluene	54	0.424	441.77	219.51	325.66	0.10	369.10	0.836	1.006	5636.44	5636.44
chlorobenzene[a]	10	0.587	472.07	301.20	408.16	0.10	0.10	0.980	1.168	61.75	51.95
chloromethane[a]	47	0.449	310.73	210.00	440.00	0.10	200.00	0.769	1.145	84.28	75.02
dichloromethane[a]	14	0.495	380.71	270.00	406.00	0.10	100.00	1.106	1.559	111.78	110.95
chloroform[a]	64	0.522	400.42	254.00	397.00	0.10	389.90	1.336	1.753	261.39	261.29
$CClF_3$	67	0.483	225.44	303.15	348.15	3.68	188.38	0.299	1.539	26.00	26.00
carbon tetrachloride	32	0.561	415.31	283.20	333.20	1.01	1475.00	1.517	1.730	415.65	415.65
trifluoromethane[a]	20	0.448	223.42	147.00	246.00	10.00	100.00	1.267	1.646	233.95	230.17
carbontetrafluoride	54	0.440	169.83	243.15	348.15	24.40	443.99	0.114	1.340	42.53	42.53
sulfurhexafluoride	44	0.497	237.90	240.00	398.00	0.63	182.70	0.088	1.850	24.53	24.49
perfluorocyclobutane	59	0.587	289.91	323.00	473.00	5.00	190.00	1.080	1.800	51.31	51.06
ammonia	27	0.373	302.81	196.90	297.84	0.10	0.10	0.602	0.733	148.24	142.27
acetone[a]	11	0.539	379.37	245.94	337.15	0.10	0.10	0.740	0.853	365.64	365.64
pyridine	47	0.542	462.79	303.15	423.15	0.10	500.00	0.862	1.106	461.75	461.57
methanol[a]	72	0.451	382.65	268.20	453.00	0.10	385.80	0.605	0.966	1923.45	1921.07
ethanol	74	0.495	383.64	263.00	437.00	0.10	265.20	0.637	0.921	2036.08	2035.57
water[a]	16	0.35	483.05	313.20	648.20	0.01	22.36	0.315	1.002	122.52	82.45
overall	1088									680.43	

[a] Data points are reduced due to obtaining negative values for diffusivity.

6. Self-Diffusivity of Nonalkanes

Although the *n*-alkanes provide a firm foundation for studying the fundamentals of diffusivity, our ultimate goal is to provide a generalized correlation for the diffusivity of any compound. In this section, we seek a generalized correlation for a database of 24 compounds compiled from the literature. The database covers the compounds listed in Table 5 and is available online as supplemental data associated with this publication. The REFPROP program[23] was used to calculate the densities when not reported.

Characterizing the reference contribution to the diffusivity requires simulation by SPEADMD as a first step. Given the reference diffusivity at individual state points, the next question is how to interpolate between state points. Subsequent to characterizing the reference system, a question arises as to the form of the attractive correction. These questions are obviated if nonalkanes can be treated as effective *n*-alkanes.

One key issue is whether the reference diffusivities can be accurately interpolated using eq 4. Equation 4 includes two parameters: m^{eff} and $C\rho D_o^{mon}$. Table 5 lists the values for m^{eff} and $C\rho D_o^{mon}$ along with the % AAD in correlating the reference simulation with eq 4. The overall deviation is 6.7% with most compounds having deviations less than 10%. The larger deviations for some compounds result primarily from scatter in the simulations, rather than systematic error, as illustrated in Figure 8. The only peculiarity is that the value of m^{eff} is less than unity for three compounds. Although peculiar, this allowance permitted correlation improvements of 2−3% AAD. The shapes of these compounds are tetrahedral (CCl_4), bipyrmidal (SF_6), and concave (C_4F_8), which are fairly unusual. Hence we expect this peculiar behavior to occur only in exceptional situations. We conclude that eq 4 is satisfactory for correlating the reference simulation results.

After the reference simulations of each compound, we would like to consider the temperature effects as defined by eqs 10 and 14. To extend eq 10 to nonalkanes, we adapt the relation between the number of segments from *n*-alkanes with

$$\sigma_{mon}{}^3 = 6v^{eff}/\{\pi^*[1 + (m^{eff} - 1)/0.11]\} \qquad (24)$$

Figure 9 illustrates the model performance for benzene and cyclohexane at $T \approx 313$ K. Dashed lines are the results with well attraction strength defined by $e_0 = 0$ and $\varepsilon^{LJ}/k_B = 79$ K. It is observed that the equivalent *n*-alkane does not quantitatively predict diffusivities of nonalkane compounds. Since benzene's diffusivity is underestimated and cyclohexane's is overestimated, there is no systematic correction that can compensate for both compounds. On the other hand, e_0 can be adjusted empirically to fit the experimental data on a compound-specific basis. In Figure 9, solid lines illustrate the results with adjusted attraction strengths of $\varepsilon/k_B = 186.8$ K for benzene and $\varepsilon/k_B = 447.1$ K for cyclohexane. This approach can also be applied to other compounds. For hydrogen bonding species, it is necessary to correct for the shift in diffusivity that occurs. As an initial approximation, we find that $e_0 = 0.2$ for alcohols and water provides a satisfactory correction at present. Table 6 includes attractive well strength values, % AAD and % bias values, and the corresponding number of data points (NDP) used in the fitting procedure are listed. With a single adjustable parameter, the SPEADMD correlation provides 19.3% AAD for 1144 data points. Table 7 shows comparisons to Liu's method using Silva's guideline for ε/k_B such that there is one adjustable parameter in each correlation. The generalized application of Liu's method provides an overall accuracy of 65.7% AAD.

7. Conclusion

In summary, we find that SPEADMD provides a viable methodology for understanding self-diffusivity behavior from a molecular perspective. Reference simulations combine with perturbation terms to correlate the effect of attractive forces. A generalized correlation is obtained that can predict *n*-alkane diffusivity at all molecular weights below the entanglement threshold. The proposed correlation was used for 35 compounds (1801 data points) over wide temperature and pressure ranges with 14% AAD overall (alkanes and nonalkanes together). The equation has been compared with available empirical correlations based on the Lennard-Jones potential. It is observed that there are drawbacks in the reliability and accuracy of correlations based on equivalent spheres or the volume conservation

assumption. The advantage of correlation based on the SPEAD-MD model is to have interaction site diameters that provide consistency with the thermodynamic description of molecule.

In the proposed correlation, a mean field attraction is applied instead of the attractive energies derived from the thermodynamic properties. There is no perturbation theory for diffusivity comparable to thermodynamic perturbation theory and simulation of the full potential at least an order of magnitude slower than the reference simulation. Instead, the values of attractive well strength are related to critical temperature. It is observed that the average deviations with this approach are reasonable. Extrapolations to higher molecular weights showed that the correlation should provide accuracy of ~15% at C30 and 25% at C60. This minor decay of precision should be expected because both the simulations and experiments are more difficult. Future work should focus on simulations with the full potential models for pure fluids to examine the reliability and accuracy of perturbation terms relative to the fundamental simulations rather than semiempirical regression from experimental data. Simulations with the full potential were conducted for square well spheres to examine the attractive effects qualitatively, but understanding the peculiar differences between benzene and cyclohexane, for example, will require more quantitative analysis.

Other future work should focus other transport properties. Preliminary work on thermal conductivity is promising with the approach used here. The Stokes−Einstein relation should provide the initial basis for a semiempirical correlation of viscosity. This correlation would be the basis of comparison for more rigorous theories and refinement of full potential simulations.

Supporting Information Available: A database containing % AAD and % bias values for 657 data points from ethane through *n*-hexadecane. This material is available free of charge via the Internet at http://pubs.acs.org.

Appendix

Table A1 shows the sample self-diffusivity prediction for

Table A1

method	eq 14	Zabaloy's correlation	Liu's correlation
$(D\rho) \times 10^{-5}$ (g/cm-s)	5.36	6.14	5.52
deviation %	9.04	4.07	–6.22

methane at 160 K and 1.649 MPa and *n*-eicosane at 0.1 MPa and $D\rho^{EXP} = 5.89 \times 10^{-5}$ g/cm-s and $\rho = 0.33652$ g/cm^3.

Literature Cited

(1) Liu, H.; Silva, C. M.; Macedo, E. A. Unified Approach to the Self-Diffusion Coefficients of Dense Fluids over Wide Ranges of Temperature and Pressure: Hard-Sphere, Square-Well, Lennard-Jones, And Real Substances. *Chem. Eng. Sci.* **1998**, *53*, 2403.

(2) Zabaloy, M. S.; Vasquez, V. R.; Macedo, E. A. Description of Self-Diffusion Coefficients of Gases, Liquids, and Fluids at High Pressure Based on Molecular Simulation Data. *Fluid Phase Equilib.* **2006**, *242*, 43–56.

(3) Yu, Y.-X.; Gao, G.-H. Self-Diffusion Coefficient Equation for Polyatomic Fluid. *Fluid Phase Equilib.* **1999**, *166*, 111–124.

(4) Kremer, K.; Grest, G. S. Dynamics of Entangled Linear Polymer Melts: A Molecular Dynamics Simulation. *J. Chem. Phys.* **1990**, *92*, 5057.

(5) Smith, S. W.; Hall, C. K.; Freeman, B. D. Molecular Dynamics Study of Transport Coefficients for Hard-Chain Fluids. *J. Chem. Phys.* **1995**, *102*, 1057.

(6) Harmandaris, V. A.; Mavrantzas, V. G.; Theodorou, D. N. Atomistic Molecular Dynamics Simulation of Polydisperse Linear Polyethylene Melts. *Macromolecules* **1998**, (31), 7934–7943.

(7) Harmandaris, V.; Mavrantzas, V.; Theodoru, D.; Kroger, M.; Ramirez, J.; Ottinger, H.; Vlassopoulos, D. Crossover from the Rouse to the Entangled Polymer Melt Regime: Signals fom Long, Detailed Atomistic Molecular Dynamics Simulations, Supported by Rheological Experiments. *Macromolecules* **2003**, *36*, 1376–1387.

(8) Mavrantzas, V. G.; Boone, T. D.; Zervopoulou, E.; Theodorou, D. N. End-Bridging Monte Carlo: A Fast Algorithm for Atomistic Simulation of Condensed Phases of Long Polymer Chains. *Macromolecules* **1999**, *32*, 5072–5096.

(9) Rowley, R. L.; Painter, M. M. Diffusion and Viscosity Equations of State for a Lennard-Jones Fluid Obtained from Molecular Dynamics Simulations. *Int. J. Therm.* **1997**, *18* (5), 1109–1121.

(10) Moore, J. D.; Cui, S. T.; Cochran, H. T.; Cummings, P. T. Rheology Of Lubricant Basestocks: A Molecular Dynamics Study Of C30 Isomers. *J. Chem. Phys.* **2000**, *113*, 8833–8840.

(11) Daivis, P. J.; D.J., E. Transport Coefficients of Liquid Butane Near the Boiling Point by Equilibrium Molecular Dynamics. *J. Chem. Phys.* **1995**, *103* (10), 4261.

(12) Dysthe, D. K.; Fuchs, A. H.; Rousseau, B. Fluid Transport Properties by Equilibrium Molecular Dynamics. I. Methodology at Extreme Fluid States. *J. Chem. Phys.* **1999**, *110* (8), 4047–4059.

(13) Dysthe, D. K.; Fuchs, A. H.; Rousseau, B., III. Evaluation of United Atom Interaction Potential Models for Pure Alkanes. *J. Chem. Phys.* **2000**, *112*, 7581–7590.

(14) Unlu, O.; Gray, N. H.; Gerek, Z. N.; Elliott, J. R. Transferable Step Potentials for the Straight Chain Alkanes, Alkenes, Alkynes, Ethers, and Alcohols. *Ind. Eng. Chem. Res.* **2004**, *43*, 1788–1793.

(15) Baskaya, F. S.; Gray, N. H.; Gerek, Z. N.; Elliott, J. R. Transferable Step Potentials for Amines, Amides, Acetates, and Ketones. *Fluid Phase Equilib.* **2005**, *236*, 42–52.

(16) Cui, J.; Elliott, J. R., Jr. Phase Diagrams for Multistep Potential Models of *n*-Alkanes by Discontinuous Molecular Dynamics/Thermodynamic Perturbation Theory. *J. Chem. Phys.* **2002**, *116*, 8625.

(17) Alder, B. J.; Gass, D. M.; Wainwright, T. E. The Transport Coefficients for a Hard-Sphere Fluid. *J. Chem. Phys.* **1970**, *53*, 3813.

(18) Sigurgeirsson, H.; Heyes, D. M. Transport Coefficients of Hard Sphere Fluids. *Mol. Phys.* **2003**, *101* (3), 469–482.

(19) Salim, P. H.; Trebble, M. A. Modified Interacting-Sphere Model for Self-Diffusion and Infinite-Dilution Mutual-Diffusivity of *N*-Alkanes. *J. Chem. Soc., Faraday Trans.* **1995**, *91*, 245–250.

(20) Doi, M. *Introduction to Polymer Physics*; Oxford Clarendon Press: New York, 1996.

(21) Tao, H.; Lodge, T. P.; von Meerwall, E. D. Diffusivity and Viscosity of Concentrated Hydrogenated Polybutadiene Solutions. *Macromolecules* **2000**, *33*, 1747–1758.

(22) von Meerwall, E. D.; Beckman, S.; Jang, J.; Mattice, W. L. Diffusion of Liquid *N*-Alkanes: Free-Volume and Density Effects. *J. Chem. Phys.* **1998**, *108*, 4299–4304.

(23) Lemmon, E. W.; McLinden, M. O.; Huber, M. L. *REFPROP -Reference Fluid Thermodynamic and Transport Properties- (NIST Standard Reference Database 23), 7*; National Institute of Standards and Technology: Gaithersburg, MD, 2002.

(24) Elliott, J. R.; Daubert, T. E. The Temperature Dependence of the Hard Sphere Diameter. *Fluid Phase Equilib.* **1986**, *31*, 153–160.

(25) Barker, J. A.; Henderson, D. Perturbation Theory and Equation of State for Fluids. II. Successful Theory of Liquids. *J. Chem. Phys.* **1967**, *47*, 4714.

(26) Weeks, J. D.; Chandler, D.; Anderson, H. C. Role of Repulsive Forces in Determining the Equilibrium Structure of Simple Liquids. *J. Chem. Phys.* **1971**, *54*, 5237.

(27) Dawson, R.; Khoury, F.; Kobayashi, R. Self-Diffusion Measurements in Methane by Pulsed Nuclear Magnetic Resonance. *AIChE J.* **1970**, *16* (5), 725–729.

(28) Harris, K. R.; Trappeniers, N. J. The Density Dependence of the Self-Diffusion Coefficient of Liquid Methane. *Physica* **1980**, *104A*, 262–280.

(29) Greiner-Schmid, A. S.; Wappmann, S.; Has, M.; Ludemann, H.-D. Self-Diffusion in the Compressed Fluid Lower Alkanes: Methane, Ethane, and Propane. *J. Chem. Phys.* **1991**, *94* (8), 5643–5649.

(30) Dymond, J. H.; Harris, K. R. The Temperature and Density Dependence of the Self-Diffusion Coefficient of *n*-Hexadecane. *Mol. Phys.* **1992**, *75* (2), 461–466.

(31) Speedy, R. J.; Prielmeier, F. X.; Vardag, T.; Lang, E. W.; Luedemann, H. D. Diffusion in Simple Fluids. *Mol. Phys.* **1989**, *66* (3), 577–590.

(32) Meier, K.; Laesecke, A.; Kabelac, S. A Molecular Dynamics Simulation Study of the Self-Diffusion Coefficient and Viscosity of the Lennard-Jones Fluid. *Int. J. Thermophys.* **2001**, *22* (1), 161–173.

(33) Liu, J.-X.; Bowman, T. L., II; Elliott, J. R. Discontinuous Molecular Dynamics Simulation of Hydrogen-Bonding Systems. *Ind. Eng. Chem. Res.* **1994**, *33* (4), 957.

(34) Michels, J.; Trappeniers, N. Molecular Dynamical Calculations of the Transport Properties of a Square-Well Fluid. V. The Coefficient of Self-Diffusion. *Physica* **1982**, *116A* (3), 516–525.

(35) Alder, B. J.; Alley, W. E.; Rigby, M. Correction to the van der Waals Model for Mixtures and for the Diffusion Coefficient. *Physica* **1974**, *73*, 143–155.

(36) Longuet-Higgins, H. C.; Valleau, J. P. Transport Coefficients of Dense Fluids of Molecules Interacting According to a Square-Well Potential. *Mol. Phys.* **1958**, *1*, 284.

(37) Davis, H. T.; Rice, S. A.; Sengers, J. V. On the Kinetic Theory of Dense Fluids. IX. The Fluid of Rigid Spheres with a Square-Well Attraction. *J. Chem. Phys.* **1961**, *35*, 2210.

(38) Karkheck, J.; Stell, G. Kinetic Perturbation Theory. Structure of Collision Integrals for the Square-Well Gas. *J. Phys. Chem.* **1983**, *87*, 2858–2868.

(39) Davis, H.; Luks, K. Transport Properties of a Dense Fluid of Molecules Interacting with a Square-Well Potential. *J. Chem. Phys.* **1965**, *69* (3), 869–880.

(40) Dufty, J. W.; Mo, K. C.; Gubbins, K. E. Models for Self-diffusion in the Square Well Fluid. *J. Chem. Phys.* **1991**, *94* (4), 3132–3140.

(41) Hoffman, D. K.; Curtis, C. F. *Phys. Fluids* **1965**, *8*, 667.

(42) Tyrell, J. J. V.; Harris, K. R. *Diffusion in Liquids*; Butterworth & Co. Ltd.: London, 1984.

(43) Chandler, D. Rough Hard Sphere Theory of the Self-diffusion Constant for Molecular Fluids. *J. Chem. Phys.* **1975**, *62*, 1358.

(44) Dymond, J. H. Hard-Sphere Theories of Transport Properties. *Chem. Soc. Rev.* **1985**, *14*, 317.

(45) Meckl, S.; Zeiler, M. D. Self-Diffusion Measurements of Ethanol and Propanol. *Mol. Phys.* **1988**, *63*, 85–95.

(46) Straub, J. E. Analysis of the Role of Attractive Forces in Self-Diffusion of a Simple Fluid. *Mol. Phys.* **1992**, *76*, 373.

(47) Heyes, D. M.; Branka, A. C. Transport Coefficients of Soft Sphere Fluids. *Phys. Chem. Chem. Phys.* **2005**, *7*, 1220–1227.

(48) Shukla, K. P. Phase Equilibria and Thermodynamic Properties of Hard Core Yukawa Fluids of Variable Range From Simulations and Analytical Theory. *J. Chem. Phys.* **2000**, *112*, 10358.

(49) Kolafa, J.; Nezbeda, I. The Lennard-Jones Fluid: An Accurate Analytic and Theoretically-Based Equation of State. *Fluid Phase Equilib.* **1994**, *100*, 1–34.

(50) Rosenfeld, Y. Relation between the Transport Coefficients and the Internal Entropy of Simple Systems. *Phys. Rev. A* **1977**, *15*, 2545.

(51) Mittal, J.; Errington, J. R.; Truskett, T. M. Relationships between Self-Diffusivity, Packing Fraction, and Excess Entropy in Simple Bulk and Confined Fluids. *J. Phys. Chem. B* **2007**, *111*, 10054–10063.

(52) Elliott, J. R.; Gray, N. H. Asymptotic Trends in Thermodynamic Perturbation Theory. *J. Chem. Phys.* **2005**, *123*, 184902.

(53) Collins, A. F.; Woolf, L. A. Self-Diffusion in Benzene under Pressure. *J. Chem. Soc.: Faraday Trans. I* **1975**, *71*, 2296.

(54) Jonas, J.; Hasha, D.; Huang, S. G. Density Effects on Transport Properties in Liquid Cyclohexane. *J. Phys. Chem.* **1980**, *84*, 109.

(55) Helbaek, M.; Hafskjold, B.; Dysthe, D. K.; Sorland, G. H. Self-Diffusion Coefficients of Methane or Ethane Mixtures with Hydrocarbons at High Pressure by NMR. *J. Chem. Eng. Data* **1996**, *41*, 598–603.

(56) Harris, K. R. The Density Dependence of the Self-Diffusion Coefficient of Methane at−50°, 25°, and 50°C. *Phys. A* **1978**, *94A* (3−4), 448–464.

(57) Robinson, R. C.; Stewart, W. E. Self-Diffusion Liquid Carbon Dioxide and Propane. *Ind. Eng. Chem. Fundam.* **1968**, *7*, 90–95.

(58) Bachl, F.; Ludemann, H.-D. Pressure and Temperature Dependence of Self-Diffusion in Liquid Linear Hydrocarbons. *Z. Naturforsch., A: Phys. Sci.* **1986**, *41a*, 963–970.

(59) Karger, N.; Vardag, T.; Ludemann, H.-D. Temperature Dependence of Self-Diffusion in Compressed Monhydric Alcohols. *J. Chem. Phys.* **1990**, *93*, 3437.

(60) Dullien, F. A. L. Predictive Equations for Self-Diffusion in Liquids: a Different Approach. *AIChE J.* **1972**, *18* (1), 62–70.

(61) Harris, K. R. Temperature and Density Dependence of the Self-Diffusion Coefficient of *n*-Hexane from 223 to 333 K and up to 400 MPa. *J. Chem. Soc., Faraday Trans.* **1982**, *78*, 2265–2274.

(62) Marbach, W.; Hertz, H. G. Self and Mutual Diffusion Coefficients of some *n*-Alkanes at Elevated Temperatures and Pressures. *Z. Phys. Chem.* **1996**, *193*, 90.

(63) Ertl, H.; Dullien, F. A. L. Self-Diffusion and Viscosity of Some Liquids as a Function of Temperature. *AIChE J.* **1973**, *19* (6), 1215–1223.

(64) Harris, K. R.; Alexander, J. J.; Goscincka, T.; Malhotra, R.; Woolf, L. A.; Dymond, J. H. The Temperature and Density Dependence of the Self-Diffusion Coefficient of Liquid *n*-Octane and Toluene. *Mol. Phys.* **1993**, *78*, 235–248.

(65) Miffin, T. R.; Bennett, C. O. Self-Diffusion in Argon to 300 atm. *J. Chem. Phys.* **1958**, *29*, 975.

(66) Durbin, L.; Kobayashi, R. Diffusion of Krypton-85 in Dense Gases. *J. Chem. Phys.* **1962**, *37*, 1643.

(67) Chen, S. H.; Postol, T. A.; Skold, K. Study of Self-diffusion in Dense Hydrogen Gas by Quasi-elastic Incoherent Neutron Scattering. *Phys. Rev. A* **1977**, *16*, 2112–2119.

(68) Woolf, L. A. Self-Diffusion in Carbon Disulphide Under Pressure. *J. Chem. Soc., Faraday Trans.* **1982**, *178*, 583.

(69) Etesse, P.; Zega, J. A.; Kobayashi, R. High Pressure Nuclear Magnetic Resonance Measurement of Spin-Lattice Relaxation and Self-Diffusion in Carbon Dioxide. *J. Chem. Phys.* **1992**, *97*, 2022.

(70) Arends, B.; Prins, K. O.; Trappeniers, N. J. Self-Diffusion in Gaseous and Liquid Ethylene. *Physica* **1981**, *107A*, 307.

(71) Baker, E. S.; D, R. B.; Jonas, J. Self-Diffusion in Compressed Supercritical Ethylene. *J. Phys. Chem.* **1984**, *88*, 5425.

(72) McCool, M. A.; Collings, A. F.; Woolf, L. A. Pressure and Temperature Dependence of the Self-Diffusion of Benzene. *J. Chem. Soc.: Faraday Trans. I* **1972**, *68*, 1489.

(73) Parkhurst, J. H. J.; Jonas, J.; Dense liquids., I. The Effect of Density and Temperature on Self-Diffusion of Tetramethylsilane and Benzene-d_6. *J. Chem. Phys.* **1975**, *63*, 2698.

(74) Prielmeier, F. X.; Ludemann, H.-D. Self-diffusion in Compressed Liquid Chloromethane, Dichloromethane, and Trichloromethane. *Mol. Phys.* **1986**, *58*, 593.

(75) Harris, K. R.; Lam, H. N.; Raedt, E.; Easteal, A. J.; Price, W. E.; Woolf, L. A. The Temperature and Density Dependence of the Self-Diffusion Coefficient and the Shear Viscosity of Liquid Trichloromethane. *Mol. Phys.* **1990**, *71*, 1205.

(76) Collins, A. F.; Mills, R. Temperature-Dependence of Self-Diffusion for Benzene and Carbon Tetrachloride. *J. Chem. Soc.: Faraday Trans. I* **1970**, *66*, 2761.

(77) Prielmeier, F. X.; Lang, E. W.; Ludemann, H.-D. Pressure Dependence of the Self-Diffusion in Liquid Trifluoromethane. *Mol. Phys.* **1984**, *52*, 1105.

(78) Khoury, F.; Kobayashi, R. Data by NMR and Representations of Self-Diffusion Coefficients in Carbon Tetrafluoride and Determination of Intermolecular Force Constants. *J. Chem. Phys.* **1971**, *55*, 2439.

(79) DeZwaan, J.; Jonas, J. Motional Dynamics of SF_6. *J. Chem. Phys.* **1975**, *63* (11), 4606.

(80) Tison, J. K.; Hunt, E. R. Self-Diffusion, Spin-Lattice Relaxation, and Density of SF_6 Near the Critical Point. *J. Chem. Phys.* **1971**, *54*, 1526.

(81) Finney, R. J.; Fury, M.; Jonas, J. Density and Temperature Dependence of Self-Diffusion and Shear Viscosity of Perfluorocyclobutane in Dense Fluid Region. *J. Chem. Phys.* **1977**, *66*, 760.

(82) O'Reilly, D. E.; Peterson, E. M.; Scheie, C. E. Self-Diffusion in Liquid Ammonia and Deuterammonia. *J. Chem. Phys.* **1973**, *58*, 4072.

(83) Fury, M.; Munie, G.; Jonas, J. Transport Processes in Compressed Liquid Pyridine. *J. Chem. Phys.* **1979**, *70*, 1260.

(84) Hurle, R. L.; Easteal, A. J.; Woolf, L. A. Self-Diffusion in Monohydric Alchols under Pressure. *J. Chem. Soc.: Faraday Trans. I* **1985**, *81*, 769–779.

(85) Mills, R. Self-Diffusion in Normal and Heavy Water in the Range 1−45°. *J. Phys. Chem.* **1973**, *77*, 685.

(86) Riazi, M. R.; Daubert, T. E. Application of Corresponding States Principles for Prediction of Self-Diffusion Coefficients in Liquids. *AIChE J.* **1980**, *26*, 386.

(87) Wang, J. H.; Robinson, C. V.; S., E. I. Self-Diffusion and Structure of Liquid Water. III. Measurement of Self-Diffusion of Liquid water with H_2, H_3, and O_{18} as Tracers. *J. Am. Chem. Soc.* **1953**, *20*, 466.

Received for review August 7, 2009
Revised manuscript received December 1, 2009
Accepted January 6, 2010

IE901247K